Effect of the inverse Langevin approximation on the solution of the Fokker–Planck equation of non-linear dilute polymer

Amine Ammar [a,b,*]

[a] *LAMPA, Arts et Métiers ParisTech, 2 Boulevard du Ronceray, BP 93525, F-49035 Angers Cedex 01, France*
[b] *UMSSDT, ENSIT, Université de Tunis, 5 Avenue Taha Hussien, Monteury 1008, Tunis, Tunisia*

ABSTRACT

The Langevin function is defined by $L(x) = \coth(x) - 1/x$. Its inverse is useful for many applications and especially for polymer science. As the inverse exact expression has no analytic representation, many approximations have been established. The most famous approximation is the one traditionally used for the finitely extensible non-linear elastic (FENE) dumbbell model in which the inverse is approximated by $L^{-1}(y) = 3y/(1 - y^2)$. Recently Martin Kröger has published a paper entitled 'Simple, admissible and accurate approximations of the inverse Langevin and Brillouin functions, relevant for strong polymer deformation and flows' (Kröger, 2015) in which he proposed approximations with very reduced error in relation to the numeric inverse of the Langevin function. The question we aim to analyze in this short communication is: when one uses the traditional approximation rather than the more accurate one proposed by Kröger is that really significant regarding the value of the probability distribution function (PDF) in the frame work of a kinetic theory simulation? If yes when we move to the upper scale by evaluating the value of the stress, can we observe a significant difference?

By making some simple 1D simulations in homogeneous extensional flow it is demonstrated in this short communication that the PDF prediction within kinetic theory framework as well as the macroscopic stress value are both affected by the quality of the approximation.

1. Introduction

The Langevin function is defined as

$$L(x) = \coth(x) - 1/x \tag{1}$$

The inverse Langevin function is used in rheology of polymer suspension and in the molecular stress function theory. It results from the non-Gaussian statistical theory of rubber elasticity as the entropic force developed by polymer chains. When chain length approaches its maximal value corresponding to a fully stretched state, the chain force tends to infinity which implies asymptotic behavior of the inverse function near the value $y = 1$. The inverse Langevin function cannot be represented in an explicit form and necessitates an approximation using some series that uses non-rational or rational functions. For that, an accurate approximation of this function can be based on a high order series expansion. A high order series expansion is an easy way to characterize a function that cannot be expressed in a closed form. There is a correlation between the number of expansion terms and the accuracy related to the convergence rate. The exact value can be sometimes difficult to attain. An example of such approaches can be found in [5] where the inverse Langevin function is represented by a Taylor series expansion around $y = 0$ based on the first four nonzero coefficients

$$L_{\text{Kuh}}^{-1}(y) = 3y + \frac{9}{5}y^3 + \frac{297}{175}y^5 + \frac{1539}{875}y^7 + O(y^9) \text{ (see [5])} \tag{2}$$

Near the singularity point $y = 1$ the Taylor series cannot still accurately describe the behavior of the inverse Langevin function. In this case, an approximation by a rational function defined as a fraction of polynomials can be advantageous since it is able to reproduce the asymptotic behavior. Some examples of approximations that can be found in the literature are listed below [6,7]:

$$L_{\text{Tre}}^{-1}(y) = \frac{3y}{1 + 0.2y^6 - 0.6y^2 - 0.2y} \text{ (see [7])} \tag{3}$$

$$L_{\text{Puso}}^{-1}(y) = \frac{3y}{1 - y^3} \text{ (see [6])} \tag{4}$$

$$L_{\text{Coh}}^{-1}(y) = y\frac{3 - y^2}{1 - y^2} \text{ (see [2])} \tag{5}$$

The most famous approximation is the one introduced by Warner in 1972 [8] traditionally called the FENE approximation.

$$L_{\text{FENE}}^{-1}(y) = \frac{3y}{(1 - y^2)} \tag{6}$$

In this work we are going to focus our attention on the traditional FENE approximation which will be referred to in the results as 'FENE'. Our attention will also be focused on the two approximations proposed by Körger in [4] that will be respectively referred to as 'Kr1' and 'Kr2'

$$L_{\text{Kr1}}^{-1}(y) = \frac{3y}{(1 - y^2)(1 + y^2/2)} \tag{7}$$

$$L_{\text{Kr2}}^{-1}(y) = \frac{3y - \frac{y}{5}(6y^2 + y^4 - 2y^6)}{(1 - y^2)} \tag{8}$$

Cohen approximation [2] had been chosen from the mentioned four approximations to be added to our illustrations because it has the best performance from this set of Eqs. (2)–(5) (as discussed in the mentioned Ref. [4]). This paper is organized as follows: first the main equations of the kinetic theory framework are recalled, then the resolution technique is briefly described and finally results are discussed.

2. Polymer kinetic theory equations

The non-rigid dumbbell model consists of two beads connected by a spring connector. The bead serves as an interaction point with the solvent, and the spring contains the local stiffness depending on local stretching (see [1] for more details).

The dynamic of the chain is governed by hydrostatic, Brownian, and connector forces. If we denote by $\dot{\mathbf{r}}_1$ and $\dot{\mathbf{r}}_2$ the velocities of the two beads located at positions $\mathbf{r}_1$ and $\mathbf{r}_2$, these three contributions can be easily identified in the three terms of each of the following equation:

$$-\zeta(\dot{\mathbf{r}}_2 - v_0 - \boldsymbol{\kappa} \cdot \mathbf{r}_2) - k_{\text{B}}T \frac{\partial}{\partial \mathbf{r}_2}(\ln \Psi) - \mathbf{F}^c = 0 \tag{9}$$

$$-\zeta(\dot{\mathbf{r}}_1 - v_0 - \boldsymbol{\kappa} \cdot \mathbf{r}_1) - k_{\text{B}}T \frac{\partial}{\partial \mathbf{r}_1}(\ln \Psi) + \mathbf{F}^c = 0 \tag{10}$$

where ζ is the drag coefficient, v is the velocity field, v_0 is an average velocity, $\boldsymbol{\kappa}$ is the velocity gradient tensor ($\kappa_{ij} = \partial v_i/\partial x_j$), k_{B} is the Boltzmann constant, T is the absolute temperature and $\Psi(\mathbf{x})$ is the probability distribution function for a dumbbell connector vector $\mathbf{x} = \mathbf{r}_2 - \mathbf{r}_1$. From Eqs. (9) and (10) we can derive the following equation:

$$\dot{\mathbf{x}} = \boldsymbol{\kappa} \cdot \mathbf{x} - \frac{2}{\zeta}\left(k_{\text{B}}T \frac{\partial}{\partial \mathbf{x}}(\ln \Psi) + \mathbf{F}^c(\mathbf{x})\right) \tag{11}$$

The connector force can take different forms leading to different kinetic models. The connector force is given by:

$$\mathbf{F}^c(\mathbf{x}) = \frac{h}{3}L^{-1}\left(\frac{x}{x_0}\right)\mathbf{x} \tag{12}$$

where $x = |\mathbf{x}|$, h is the spring coefficient and x_0 is the maximum spring length. A particularity of this model is that there is no closure approximation able to substitute the microscopic description by an equivalent constitutive macroscopic equation [3]. The associated evolution of the distribution function can be written as:

$$\frac{\partial \Psi}{\partial t} = -\frac{\partial}{\partial \mathbf{x}} \cdot \left\{ \left(\boldsymbol{\kappa} \cdot \mathbf{x} - \frac{2}{\zeta}\mathbf{F}^c(\mathbf{x})\right) \Psi \right\} + \frac{2k_{\text{B}}T}{\zeta} \frac{\partial^2 \Psi}{\partial \mathbf{x}^2} \tag{13}$$

The problem defined by Eq. (13) has a characteristic relaxation time $\theta = \zeta/4h$ and a dimensionless finite extensibility parameter $b = hx_0^2/k_{\text{B}}T$. Thus vector $\mathbf{x}$ can be made dimensionless with $\sqrt{k_{\text{B}}T/h}$, $\boldsymbol{\kappa}$ with $1/\theta$ (so it can be viewed as a Weissenberg number We), time with θ and the polymer stress tensor with $n_c k_{\text{B}}T$ where

n_c is the number of chains in a unit volume. Consequently, the dimensionless form of problem (13) writes:

$$\frac{\partial \Psi}{\partial t} = -\frac{\partial}{\partial \mathbf{x}} \cdot \left\{ \left(\boldsymbol{\kappa} \cdot \mathbf{x} - \frac{1}{2}H(x)\mathbf{x}\right) \Psi \right\} + \frac{1}{2} \frac{\partial^2 \Psi}{\partial \mathbf{x}^2} \tag{14}$$

where $H(x)$ becomes the dimensionless connector force, that in the FENE model results:

$$H_{\text{FENE}}(x) = \frac{1}{1 - x^2/b} \tag{15}$$

In order to take into account the Kröger approximations this expression becomes

$$H_{\text{Kr1}}(x) = \frac{1}{(1 - x^2/b)(1 + x^2/(2b))} \tag{16}$$

or

$$H_{\text{Kr2}}(x) = \frac{1 - \frac{1}{15}(6x^2/b + x^4/b^2 - 2x^6/b^3)}{1 - x^2/b} \tag{17}$$

And in the same way the Cohen approximation gives the following function:

$$H_{Coh}(x) = \frac{1 - x^2/(3b)}{1 - x^2/b} \tag{18}$$

To be able to evaluate exactly the accuracy of these approximations we are going to establish a reference solution using the exact inverse of the Langevin function. In this case the function $H_{Exact}(x)$ will be calculated using a Newton's method. Another alternative consists to use the analytic (but long expression) for an excellent approximation to the exact inverse Langevin which is in [4]. These two approaches gives exactly the same results.

Moreover, a normalization condition is associated with the probability distribution:

$$\int \Psi(\mathbf{x}) \, d\mathbf{x} = 1 \tag{19}$$

Finally, the relation between statistical distribution of dumbbell configurations and the polymer stress $\boldsymbol{\tau}_p$ is provided by Kramers expression [1]

$$\boldsymbol{\tau}_p = \langle H(x) \, \mathbf{xx} \rangle - \mathbf{I} = \int \Psi(\mathbf{x})(H(x)\mathbf{xx}) \, d\mathbf{x} - \mathbf{I}. \tag{20}$$

$\mathbf{I}$ being the unit tensor (takes the value 1 in the 1D case).

We must notice with respect to Eq. (14) that this equation defines the time evolution of the distribution function, whose integration requires to specify the initial distribution denoted by Ψ_0. Thus, a reasonable choice lies in taking as initial distribution the equilibrium steady state related to a null velocity gradient. That distribution can be obtained by solving the following equation:

$$\frac{\partial}{\partial \mathbf{x}} \cdot \left\{ \left(\frac{1}{2}H(x) \, \mathbf{x}\right) \Psi_0 \right\} + \frac{1}{2} \frac{\partial^2 \Psi_0}{\partial \mathbf{x}^2} = 0 \tag{21}$$

The resulting distribution Ψ_0 will be considered as the initial condition.

3. Finite Element resolution technique

We consider simple flows characterized by homogeneous velocity gradients, which implies that the previous material derivative reduces to the partial derivative. Taking into account the homogenous gradient of velocity, no discretization in physical variables is required, and therefore, we proceed by discretizing with respect to the conformation coordinates.

$$\frac{\partial \Psi}{\partial t} + E_0(\mathbf{x})\Psi + E_1(\mathbf{x}) \frac{\partial \Psi}{\partial \mathbf{x}} - \frac{1}{2} \frac{\partial^2 \Psi}{\partial \mathbf{x}^2} = 0 \tag{22}$$
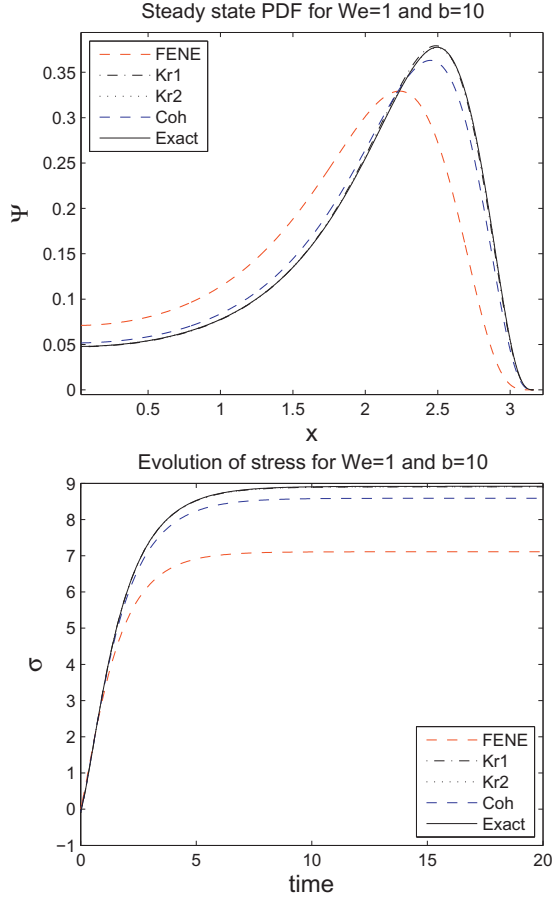
Fig. 1. Steady state PDF and transient stress for $We = 1$ and $b = 10$.
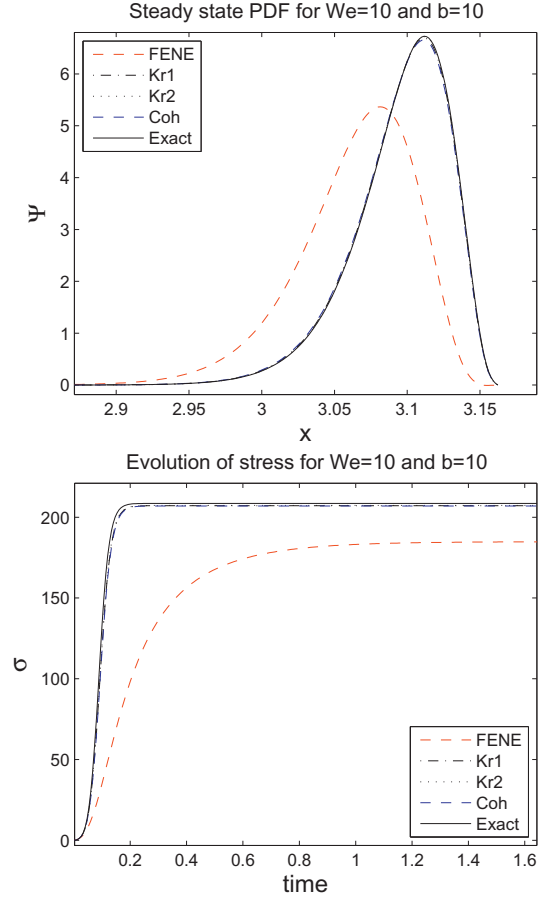

Fig. 2. Steady state PDF and transient stress for $We = 10$ and $b = 10$.

From a practical point of view, the configuration domain Ω is bounded. This domain is chosen such that the distribution function can be assumed vanishing on its boundary. Firstly, the problem is formulated in the Finite Element framework using a weighting function Ψ^*

$$\int_\Omega \Psi^* \frac{d\Psi}{dt} d\Omega + \int_\Omega \Psi^* E_0(\mathbf{x}) \Psi d\Omega$$
$$+ \int_\Omega \Psi^* E_1(\mathbf{x}) \frac{\partial \Psi}{\partial \mathbf{x}} d\Omega - \int_\Omega \frac{1}{2} \Psi^* \frac{\partial^2 \Psi}{\partial \mathbf{x}^2} d\Omega = 0$$

where

$$E_0(\mathbf{x}) = \frac{\partial}{\partial \mathbf{x}} \cdot \left(\kappa \cdot \mathbf{x} - \frac{1}{2}\mathbf{x}H(x) \right)$$

$$E_1(\mathbf{x}) = \kappa \cdot \mathbf{x} - \frac{1}{2}\mathbf{x}H(x)$$

The Galerkin Finite Element discretization writes

$$\Psi(\mathbf{x}) = \sum_{i=1}^{n} N_i(\mathbf{x}) \Psi_i \qquad (24)$$

where n is the total number of nodes, N_i are compact support shape functions for each node i. They take the value 1 for the node i and vanish for all other nodes (see for example [9] for more details). Due to the advection–diffusion character of Eq. (23) an appropriate stabilization of the Finite Element scheme is needed to avoid numerical instabilities induced by the convection term. An upwinding formulation is considered here, which modifies the weighting function

$$\Psi^*(\mathbf{x}) = \sum_{i=1}^{n} \overline{N}_i(\mathbf{x}) \Psi_i \qquad (25)$$

with

$$\overline{N}_i(\mathbf{x}) = N_i(\mathbf{x}) + \frac{\beta \Delta x}{2} \frac{E_1(\mathbf{x})}{|E_1(\mathbf{x})|} \cdot \frac{\partial N_i}{\partial \mathbf{x}}(\mathbf{x}) \qquad (26)$$

β is related to the local Peclet number and given by

$$\beta = \coth(\text{Pe}) - \frac{1}{\text{Pe}} \qquad (27)$$

where the local Peclet number is calculated by

$$\text{Pe} = |E_1(\mathbf{x})|\Delta x \qquad (28)$$

Δx being the local distance between two nodes of the mesh. The integration of Eq. (23) allows to obtain a linear system that has to be solved at each time step.

$$\underline{\Psi}^{*T} \mathbb{M} \underline{\dot{\Psi}} + \underline{\Psi}^{*T} \mathbb{G} \underline{\Psi} = 0 \qquad (29)$$

where

$$\mathbb{M}_{ij} = \int_\Omega N_i(\mathbf{x}) N_j(\mathbf{x}) d\Omega$$

$$\mathbb{G}_{ij} = \int_\Omega E_0(\mathbf{x}) N_i(\mathbf{x}) N_j(\mathbf{x}) + E_1(\mathbf{x}) N_i(\mathbf{x}) \frac{\partial \overline{N}_j(\mathbf{x})}{\partial \mathbf{x}}$$
$$+ \frac{1}{2} \frac{\partial N_i(\mathbf{x})}{\partial \mathbf{x}} \frac{\partial N_j(\mathbf{x})}{\partial \mathbf{x}} d\Omega$$

In the framework of an Euler implicit time integration scheme with a time step Δt, the updating of the PDF can be done using:

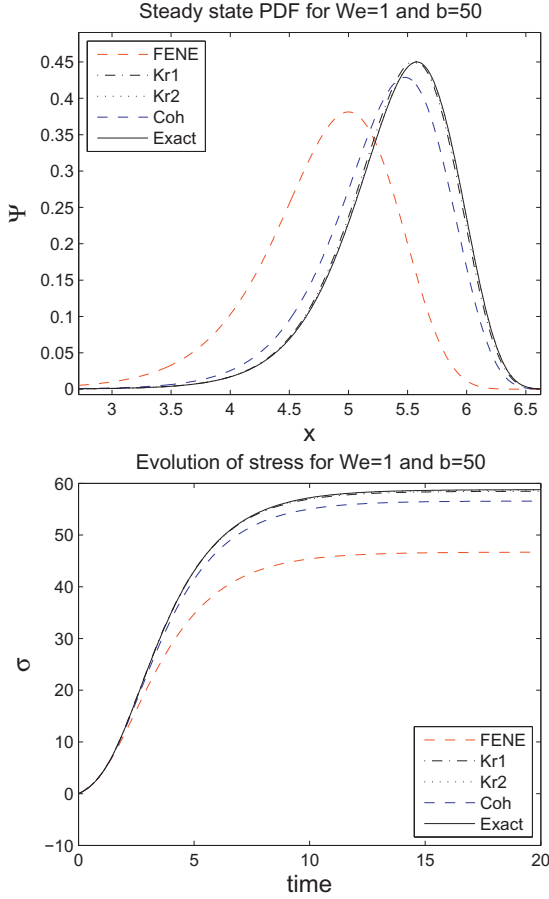$$\Psi^{t+\Delta t} = (\mathbb{M} + \Delta t \mathbb{G})^{-1} \mathbb{M} \Psi^t \qquad (30)$$

Fig. 3. Steady state PDF and transient stress for $We = 1$ and $b = 50$.

4. Results and discussion

The two parameters used in the simulation are the Weissenberg number We and the parameter characterizing the chain length b. Two values are considered for the Weissenberg number ($We = 1$ and 10) and also for the parameter b ($b = 10$ and 50). Hence, four parameter combinations are considered. In all of the results presented below the two approximations 'Kr1' and 'Kr2' are found to be similar and very close to the exact solution. For the PDF steady state and the transient stress the representations related to both Kröger's models are practically identical to the exact model. The Cohen model exhibits small differences. However the behavior of the FENE model (the dashed line) is fundamentally different.

In the following figures it is impossible to distinguish between the 'Exact', the 'Kr1' and the 'Kr2' curves as they are practically superposed. Fig. 4 shows a zoomed view in order to highlight the differences between the curves.

Fig. 1 shows that for $We = 1$ and $b = 10$ the PDF steady state solution exhibits a notable error with the FENE approximation. The extreme value of the FENE curve is lower and shifted to the left in relation to the other models. Also the steady state stress value shows a relative difference of the order of 20% compared to the exact value.

When the Weissenberg number is increased ($We = 10, b = 10$) as shown in Fig. 2, the same tendency is observed in the PDF steady state solution. But a fundamental difference in the transient stress can be seen. In fact when looking at the time interval between 0.1 and 0.3 a notable difference in the slope of the curves for the FENE model and the others can be seen. This shows how
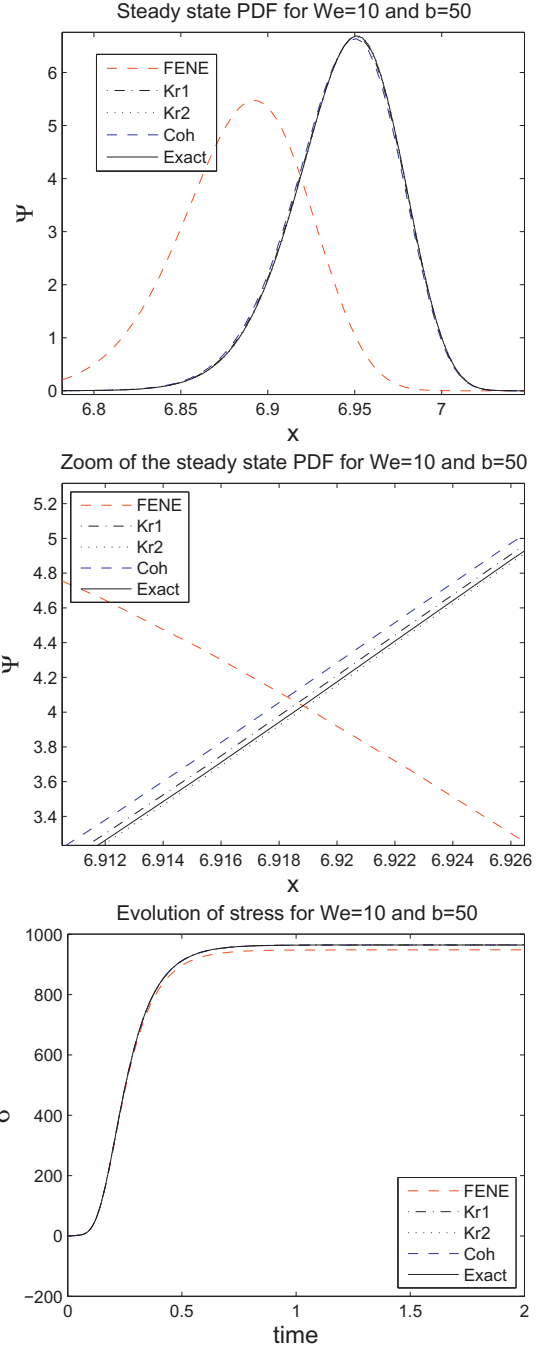

Fig. 4. Steady state PDF, zoom of the PDF and transient stress for $We = 10$ and $b = 50$.

the quality of the inverse approximation can significantly modify the apparent relaxation time and gives a warning concerning the use of the FENE approximation in similar conditions.

For Figs. 3 and 4 simulations have been performed with $We = 1, 10$ and $b = 50$. It can be observed that when the value of b is increased, the FENE shift in the PDF curves becomes more pronounced. Although the tendency in the stress evolution seems to be similar, the value of the steady state relative error remains large (of the order of 20% for $We = 1$). As some of the simulations results are similar, an accurate estimation of the error for the different models is made using two numerical criteria: the first one is related to the difference in the steady state PDFs and the second one is related to the extra stress value (characterizing the

Table 1
Comparison of errors on the PDF for the different approximations.

Err_Ψ	$We = 1$, $b = 10$	$We = 10$, $b = 10$	$We = 1$, $b = 50$	$We = 10$, $b = 50$	$We = 100$, $b = 50$	$We = 0.1$, $b = 50$
FENE	34.38	59.16	75.95	100.0	99.29	1.013
Kr1	1.027	1.003	2.894	0.803	0.103	0.146
Kr2	0.247	0.439	0.807	0.394	0.050	0.089
Cohen	6.382	1.805	15.76	2.433	0.265	0.239

Table 2
Comparison of errors on the stress value for the different approximations.

Err_τ	$We = 1$, $b = 10$	$We = 10$, $b = 10$	$We = 1$, $b = 50$	$We = 10$, $b = 50$	$We = 100$, $b = 50$	$We = 0.1$, $b = 50$
FENE	20.27	11.36	20.56	1.696	3.160	3.695
Kr1	0.169	0.674	0.519	0.010	0.033	0.039
Kr2	0.119	0.609	0.166	0.004	0.027	0.616
Cohen	3.706	0.763	3.738	0.030	0.036	1.198

macroscopic scale). The two error definitions are:

$$Err_\Psi = 100 \frac{\sqrt{\int_\Omega (\Psi^\infty_{\text{FENE, Kr1, Kr2, Coh}} - \Psi^\infty_{\text{Exact}})^2 d\Omega}}{\sqrt{\int_\Omega (\Psi^\infty_{\text{Exact}})^2 d\Omega}} \qquad (31)$$

$$Err_\tau = 100 \frac{|\tau_{\text{FENE,Kr1,Kr2,Coh}} - \tau_{\text{Exact}}|}{\tau_{\text{Exact}}} \qquad (32)$$

The calculation of these errors is summarized in Tables 1 and 2. The two error estimations, in terms of stress and PDF, show generally the same tendencies and confirm the previously discussed conclusions.

In order to observe the effect of the *We* number limit values two columns have been added to Tables 1 and 2. These columns show the results of simulations with $b = 50$ and $We = 100, 0.1$.

This limit analysis confirms the previous simulations and confirms the robustness of Kröger's approximation in relation to the FENE one. The Cohen approximation in this different case seems to be acceptable although it does not exceed Kröger's approximations in terms of accuracy.

5. Conclusion

The analysis of the FENE approximation for dilute polymer kinetic theory confirms its poor quality in terms of the PDF prediction as well as in terms of stress calculation. This could be harmful when this model is used in a micro-macro simulation. For all those who are interested in computational rheology it is henceforth recommended to use one of the two approximations provided by Eq. (7) or (8) that are not much more expensive to write or to implement than Eq. (6).

References

[1] R.B. Bird, C.F. Curtiss, R.C. Armstrong, O. Hassager, Dynamics of polymeric liquids, Kinetic Theory, vol. 2, John Wiley & Sons, 1987.
[2] A. Cohen, A Padé approximant to the inverse Langevin function, Rheol. Acta 30 (1991) 270–273.
[3] R. Keunings, On the Peterlin approximation for finitely extensible dumbells, J. Non-Newton. Fluid Mech. 68 (1997) 85–100.
[4] M. Kröger, Simple, admissible, and accurate approximants of the inverse Langevin and Brillouin functions, relevant for strong polymer deformations and flows, J. Non-Newton. Fluid Mech. 223 (2015) 77–87.
[5] W. Kuhn, F. Grun, Beziehungen zwischen elastischen Konstanten und Dehnungsdoppelbrechung hochelastischer Stoffe, Kolloid-Z. 101 (1942) 248–271.
[6] M. Puso, Mechanistic constitutive models for rubber elasticity and viscoelasticity, University of California, Davis, 2003 (Ph.D. thesis).
[7] L. Treloar, The Physics of Rubber Elasticity, Oxford University Press Inc., New York, 1975.
[8] H.R. Warner, Kinetic theory and rheology of dilute suspensions of finitely extendible dumbbells, Ind. Eng. Chem. Fundam. 11 (1972) 379–387.
[9] O.C. Zienkiewicz, R.L. Taylor, J.Z. Zhu, The Finite Element Method: Its Basis And Fundamentals, Butterworth-Heinemann Ltd., 2005.